PCCP

Cite this: *Phys. Chem. Chem. Phys.*, 2011, **13**, 17676–17682

www.rsc.org/pccp

PAPER

Self-assembled monolayer of graphene/Pt as counter electrode for efficient dye-sensitized solar cell†

Feng Gong, Hong Wang and Zhong-Sheng Wang*

Received 8th August 2011, Accepted 15th August 2011
DOI: 10.1039/c1cp22542a

Monolayer of PDDA/graphene/PDDA/H_2PtCl_6 is fabricated on conductive glass using electrostatic layer-by-layer self-assembly technique, which is then converted to graphene/Pt monolayer for use as counter electrode in dye-sensitized solar cell (DSSC). As compared to the sputtered Pt counter electrode, the self-assembled monolayer reduces the Pt amount by about 1000-fold but exhibits comparable photovoltaic performance. This finding provides a new route to fabrication of cheap and efficient counter electrodes for flow-line production of DSSCs.

1. Introduction

Owing to their high efficiency for generating electricity from solar energy and low production cost, dye-sensitized solar cells (DSSCs) have aroused extensively scientific and industrial interests and have evolved as potential alternatives to the conventional silicon solar cells in the past two decades.[1–3] Generally, the DSSC has a sandwich structure made up of a photoanode and a platinized counter electrode (CE) with a redox couple (*e.g.* I^-/I_3^-) electrolyte filling in the inter-electrode space. The photoanode comprises a porous TiO_2 nanocrystalline film sensitized by dye molecules. The operational principle of the DSSC involves the photoexcitation of the sensitizer, followed by ultrafast electron-injection into the conduction band of the semiconductor film. The dye molecule is regenerated by I^-, which is oxidized to I_3^- and then restored through the reduction of I_3^- at the CE/electrolyte interface. The electrolyte constitutes the internal conducting channel, and conduction occurs *via* the diffusion of I^- and I_3^- ions between the TiO_2 film and the CE.[4,5] The CE plays a crucial role in DSSCs, which catalyzes the reduction of I_3^- ions and relays the electrons to the electrolyte.[6] The conventional catalytic material is platinum (Pt) attributed to its outstanding conductivity, catalytic activity and stability when contacting with the iodine-based electrolyte. The sputtered Pt is often used for fabrication of high-efficiency DSSCs, but a large amount of such deposited Pt is located inside the film and does not fully function as catalyst, leading to a waste of Pt.[7] The high price of Pt and the high cost of magnetron sputtering technology undoubtedly limit its application for large-scale production of DSSCs. Therefore, search for a high-performance CE with low Pt loading using a simple and cost-effective fabrication technique is a big challenge for massive production of DSSCs.

Drop casting of chloroplatinic acid (H_2PtCl_6) on the conductive glass followed by thermal decomposition is a simple method for preparing CEs with lower Pt dosage.[8] However, thermally decomposed Pt adheres to the conductive glass weakly and disperses inhomogeneously on the substrate surface, which results in lower performance of DSSCs. In addition to the drop-casted Pt, a series of carbonaceous materials have been utilized as CEs, such as activated carbon,[9,10] carbon black,[11,12] graphite,[13–15] carbon nanotube[16–19] and graphene.[20–23] Also, some conductive polymers, such as poly (3,4-alkylenedioxythiophene),[24–26] polyaniline,[27–30] polypyrrole,[31] have been introduced into DSSCs to replace platinized CE. Yet, much lower energy conversion efficiency was obtained due to their lower conductivity and electrocatalytic activity as compared to the Pt electrode.[32] Recently, Pt dispersed on multi-wall carbon nanotubes[33] have been investigated and employed as CE in DSSCs, and promising results have been achieved.

Graphene, composed of one-atom-thick planar sheets of sp^2-bonded carobon atoms with a two-dimensional honeycomb structure, is an exceedingly promising material in many technological fields such as nanoelectronics, sensors, nanocomposites, batteries, supercapacitors and hydrogen storage.[34,35] Owing to its ubiquitous electronic properties and remarkably high electron mobility, graphene has been studied for use in fuel cells.[36–39] Herein, we demonstrate a facile approach of constructing ultrathin films on the conductive glass as a transparent and high-performance CE through electrostatic layer-by-layer self-assembly (ELSA) based on poly(diallyldimethylammonium chloride) (PDDA), graphene and H_2PtCl_6. The self-assembled film is then converted to graphene/Pt film after sintering, which performs very well as CE and is comparable to the

Department of Chemistry & Lab of Advanced Materials, Fudan University, 2205 Songhu Road, Shanghai 200438, PR China. E-mail: zs.wang@fudan.edu.cn; Fax: +86-21-5163-0345; Tel: +86-21-5163-0345

† Electronic supplementary information (ESI) available: AFM image of self-assembled graphene nanosheets and a plot of FF against the total resistance. See DOI: 10.1039/c1cp22542a

sputtered Pt in solar cell performance. This simple process for fabricating high-performance and low-cost CE of DSSCs should have a bright prospect for flow-line operation and massive production of DSSCs.

2. Experimental

2.1 Materials

Natural graphite powder, H_2PtCl_6, PDDA, LiI, I_2, 4-*tert*-butylpyridine (TBP) and 1,2-dimethyl-3-n-propylimidazolium iodide (DMPII) were obtained from Acros and Sigma–Aldrich, and these chemicals were used as received. Acetonitrile and *tert*-butylalcohol (Sinopharm Chemical Reagent Co. Ltd., China) were dehydrated using standard processes. Conductive glass (fluorine-doped SnO_2, FTO, 15Ω/square, transmittance 85%) was purchased from Nippon Sheet Glass Co., Japan. Cis-di(isothiocyanato)-bis-(2,2′-bipyridyl-4,4′-dicarboxylato) ruthenium(II) bis-tetrabutylammonium (the so-called N719) was received from Lumtec Corp., Taiwan, P. R. China and used without purification. All of other solvents and chemicals used in this study were of reagent grade, obtained from Sinopharm Chemical Reagent Co. Ltd., China, and used as received. Unilamellar graphene nanosheets (GNS) were synthesized from natural graphite powder *via* the modified Hummers method as described in previous reports.[35,40,41]

2.2 Preparation of counter electrodes and DSSCs

Self-assembled ultrathin films were constructed on the substrate (FTO or quartz) by a typical ELSA procedure,[42] as shown in Scheme 1. The cleaned substrates were dipped in a PDDA aqueous solution containing 0.5 M NaCl, which was adjusted to pH = 9 with tetramethylammonium hydroxide solution, for 20 min to get a positively charged surface, and then rinsed with ultrapure water and dried in a nitrogen gas flow. The ultrathin layers of PDDA/GNS and PDDA/$[PtCl_6]^{2-}$ were fabricated by immersing the substrates coated with PDDA in a GNS aqueous suspension (~0.015 wt%, pH = 10) or a H_2PtCl_6 (2 mM in ethanol) solution for 20 min, respectively. The ultrathin film of PDDA/GNS/PDDA/$[PtCl_6]^{2-}$ was obtained by dipping the substrate loaded with PDDA/GNS in PDDA and H_2PtCl_6 solutions sequentially. Multilayer films of $(PDDA/GNS/PDDA/[PtCl_6]^{2-})_n$ were obtained by repeating the ELSA cycles as shown in Scheme 1. Four kinds of self-assembled films of PDDA, PDDA/GNS, PDDA/$[PtCl_6]^{2-}$ and PDDA/GNS/PDDA/$[PtCl_6]^{2-}$ on FTO glass were converted to FTO, FTO/GNS, FTO/Pt, and FTO/GNS/Pt, after annealing at 350 °C for 30 min, for use as CEs in DSSCs. For comparison, the drop-casted Pt made by thermal decomposition of H_2PtCl_6 at 350 °C for 30 min and the sputtered Pt mirror (200 nm thick) were also fabricated and studied at the same conditions.

TiO_2 films (6 or 15 μm thick) were coated on FTO glass using a screen-printing method with a paste consisting of TiO_2 nanoparticles (~20 nm diameter) prepared according to a previous paper.[43] TiO_2 films were soaked overnight in the N719 solution (0.3 mM in a mixed solvent of acetonitrile and *tert*-butanol by a volume ratio of 1 : 1). The dye-loaded TiO_2 film as the working electrode and the CE were separated by a hot-melt Surlyn film (30 μm thick) and sealed together by hot-pressing. The redox electrolyte (0.1 M LiI, 0.05 M I_2, 0.6 M DMPII, and 0.5 M TBP using anhydrous acetonitrile as a solvent) was injected into the interspace between the photoanode and CE through a predrilled hole. Finally, the hole was sealed with a Surlyn film covered with a thin glass slide under heat.

2.3 Characterizations

UV-vis absorption spectra of the self-assembled films on quartz glass were recorded on a Shimadzu UV-2500 UV-Vis spectrometer. The Pt loading of the as-prepared electrodes was detected by an inductively couple plasma-atomic emission spectrometer (ICP-AES, Thermo Electron Corporation Adv. ER/S). Before the ICP measurements, the platinized CEs were immerged in aqua regia with agitation for 24 h to dissolve Pt loaded on the substrate.[7] The field emission scanning electron microscopy (FESEM S-4800, Hitachi) and atomic force microscopy (AFM, SPM-9500J3, Shimadzu) were employed to study the morphologies of the CEs. To investigate the catalytic activity and electrochemical behavior of the various CEs for the I^-/I_3^- system, electrochemical impedance spectroscopy (EIS) and cyclic voltammetry (CV) were carried out on an electrochemical workstation (ZAHNER ZENNIUM CIMPS-1, Germany). Symmetrical sandwich cells filled with the redox electrolyte (0.25 cm^2 in area and 30 μm in thickness) between two identical CEs were fabricated and used for the EIS and CV measurements.[22,44]

The current density-voltage (*J-V*) characteristics of DSSCs were recorded on a Keithley 2400 source meter under the

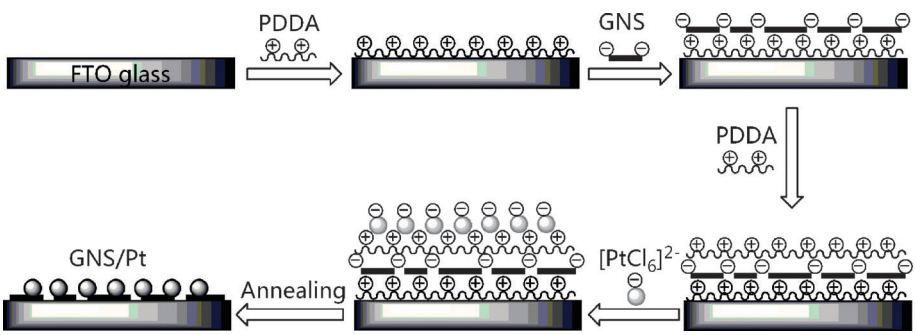

Scheme 1 Fabrication procedures of ELSA films.

illumination of AM1.5G simulated solar light coming from a solar simulator (Oriel-91193 equipped with a 1000 W Xe lamp and an AM1.5 filter), and light intensity was calibrated using a reference Si solar cell (Oriel-91150). The DSSC was fully covered with a black mask with aperture area of 0.2304 cm^2 to avoid stary light during measurements.

3. Results and discussion

3.1 Growth of self-assembled films

Fig. 1(a) shows the UV-vis absorption spectra for different self-assembled films on quartz slide. PDDA has no absorption in the measured spectral range, while PDDA/$[PtCl_6]^{2-}$ has two absorption peaks at 201 and 270 nm due to $[PtCl_6]^{2-}$. The spectral profile of PDDA/GNS having an absorption peak at 270 nm is similar to that of its aqueous suspension.[35,45] The higher baseline is attributed to the reflectance of the GNS on the substrate surface. The multilayer build-up process of $(PDDA/GNS/PDDA/[PtCl_6]^{2-})_n$ (n = 1–10) was monitored with a UV-vis absorption spectrum of the film after each deposition cycle as shown in Fig. 1(b). The composite film of PDDA/GNS/PDDA/$[PtCl_6]^{2-}$ demonstrates a peak at 270 nm, and the peak absorbance is the sum of those for $[PtCl_6]^{2-}$ and graphene. A nearly linear increase in peak absorbance as depicted in the inset of Fig. 1(b) strongly indicates a regular growth of the multilayer assembly and suggests an almost equal amount of $[PtCl_6]^{2-}$ and graphene in each layer. After annealing at 350 °C, the PDDA/GNS film does not show change in the absorption spectrum, while the peak at 270 nm for the PDDA/$[PtCl_6]^{2-}$ film disappears, indicating that graphene is stable and $[PtCl_6]^{2-}$ is converted to Pt particles upon heating. Therefore, it is concluded that the four self-assembled films on FTO (FTO/PDDA, FTO/GNS, FTO/$[PtCl_6]^{2-}$, PDDA/GNS/PDDA/$[PtCl_6]^{2-}$) are respectively converted to FTO, FTO/GNS, FTO/Pt, and FTO/GNS/Pt upon heating at 350 °C. The annealed self-assembled films were used as CEs for EIS and CV measurements and construction of DSSCs.

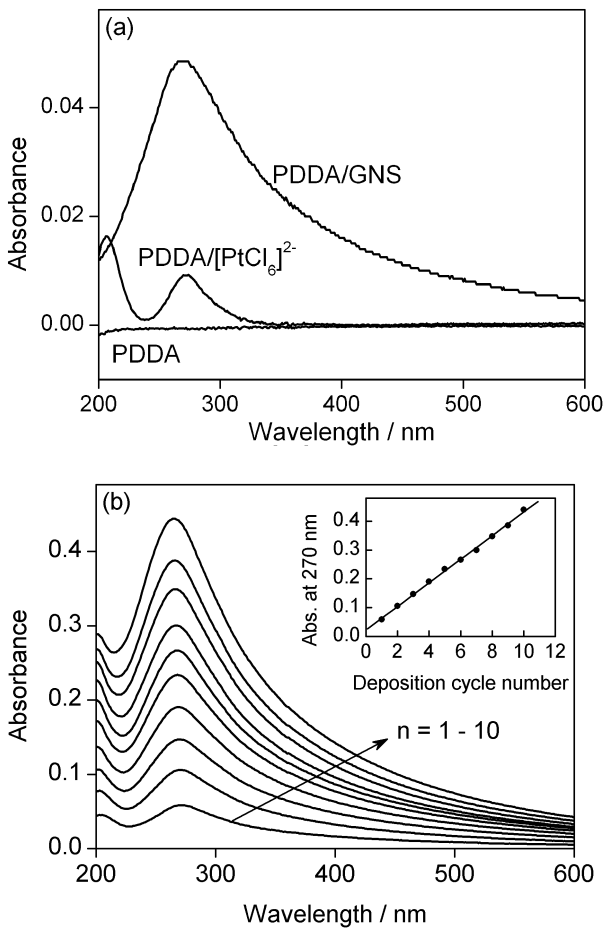

Fig. 1 UV-vis absorption spectra of (a) PDDA, PDDA/GNS, PDDA/$[PtCl_6]^{2-}$ and (b) $(PDDA/GNS/PDDA/[PtCl_6]^{2-})_n$ (n = 1–10). The inset in Fig. 1 (b) gives the plot of the absorbance at 270 nm *vs.* the number of deposition cycles.

3.2 Morphology of self-assembled films

Fig. S1 shows the tapping mode AFM image for PDDA/GNS film deposited on a mica sheet after annealing at 350 °C. The substrate was covered with monolayer of graphene with several μm in lateral dimension and <1 nm in thickness.

The morphological characteristics of these self-assembled layers after annealing were studied by FESEM, as shown in Fig. 2. Fig. 2(a) demonstrates a typical surface morphology of

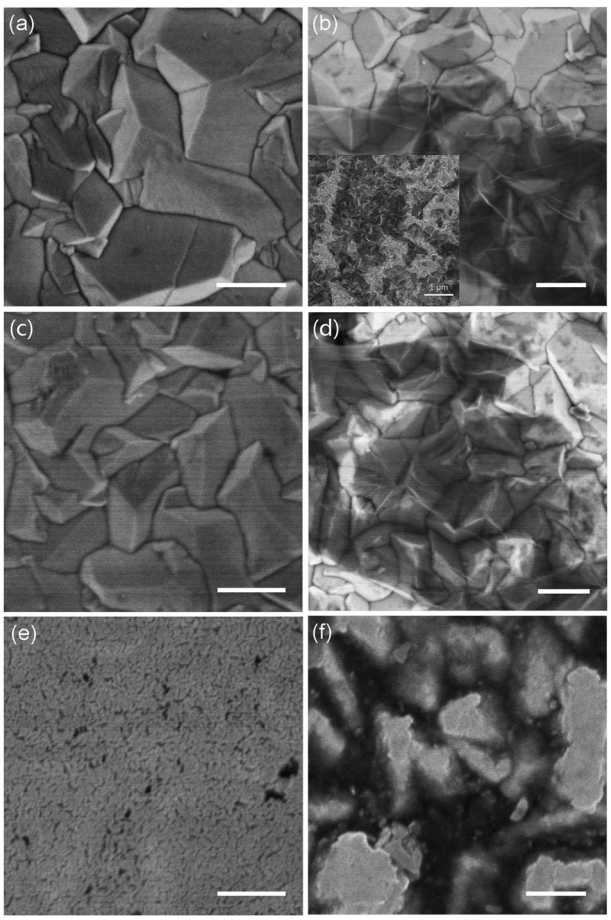

Fig. 2 Top-view SEM images of the different CEs: (a) FTO, (b) FTO/GNS; the inset gives a large-scale image, (c) FTO/Pt, (d) FTO/GNS/Pt, (e) drop-casted Pt and (f) sputtered Pt. Scale bar = 200 nm except the inset of (b).

FTO. Fig. 2(b) shows the image of graphene on FTO, where crumpled GNS mantling the FTO surface can be clearly observed. The deposition of Pt on FTO *via* self-assembly gives a SEM image in Fig. 2(c), where Pt particles cannot be observed within the SEM resolution due to the tiny size. When Pt particles are deposited on top of graphene, they are also unobservable due to the tiny size while graphene with crimples was still clearly observed, as shown in Fig. 3(d). The drop-casted Pt displays a porous morphology consisting of plentiful Pt clusters as seen in Fig. 3(e). Massive Pt bulks can be seen in Fig. 3(f) for the sputtered Pt, and the SnO_2 layer in FTO are no longer observed due to the full and thick coverage of Pt.

Pt loading amount is a restraining factor of the device cost and determines the catalytic activity. ICP-AES measurement reveals that the sputtered Pt has the highest Pt loading up to 308.9 μg cm^{-2}, and the drop-casted Pt has 23.0 μg cm^{-2}. On the contrary, the FTO/Pt and FTO/GNS/Pt only contain Pt with 0.3–0.4 μg cm^{-2}. Obviously, the self-assembled FTO/Pt and FTO/GNS/Pt contain much smaller amount of Pt than the sputtered and drop-casted Pt counter electrodes.

3.3 Catalytic activity evaluated by EIS

The resistances and the catalytic activity of the CE on the charge transfer process have great effect on the performance of DSSCs. A high-performance CE should have a low resistance and high catalytic activity. To evaluate the properties of the annealed self-assembled films as CEs in DSSCs, EIS analysis was carried out with a symmetric cell to eliminate the influence of the photoanode. A Randles-type circuit (Fig. 3(a)) is adopted to estimate the resistance for a symmetric cell.[21,22,43]

Fig. 3(b–d) illustrates the Nyquist plots of the symmetric cells with different CEs, in which the high-frequency intercept on the real axis represents the series resistance (R_s) and the charge-transfer resistance (R_{ct}) at the CE interface can be estimated from half the value of the real semicircle.[8] R_s and R_{ct} are usually used to mainly describe the resistance of the substrate and the catalytic activity of the electrode for reducing triiodide ions, respectively.[10] The measured R_s of 6.8 Ω for FTO is similar to the resistance of FTO. The large R_{ct} value (3553.0 Ω) for FTO indicates its very poor catalytic activity. Deposition of GNS on the FTO surface *via* self-assembly does not influence R_s significantly, but decreases R_{ct} by about 3-fold. This result indicates that graphene has better catalytic activity than FTO but is still poor judged from the high R_{ct} value. Tiny Pt particles deposited on FTO *via* self-assembly decreases R_{ct} remarkably to 46.4 Ω, indicating its better catalytic activity than graphene. The deposition of Pt on top of graphene *via* self-assembly further lowers the R_{ct} to 7.7 Ω. As the FTO/Pt and FTO/GNS/Pt films contain almost same amount of Pt, it is thus interesting that the latter exhibits much better catalytic activity than the former. The distinction of the self-assembled FTO/Pt and FTO/GNS/Pt comes from the middle GNS. It is easy to comprehend that part of Pt particles are entrapped in ravines of FTO layer, which leads to less contact of Pt with electrolyte and hence larger R_{ct}. When graphene is first deposited on the FTO surface, it can serve as scaffolds of Pt particles, thus increasing the effective contact of Pt with the electrolyte and reducing R_{ct}

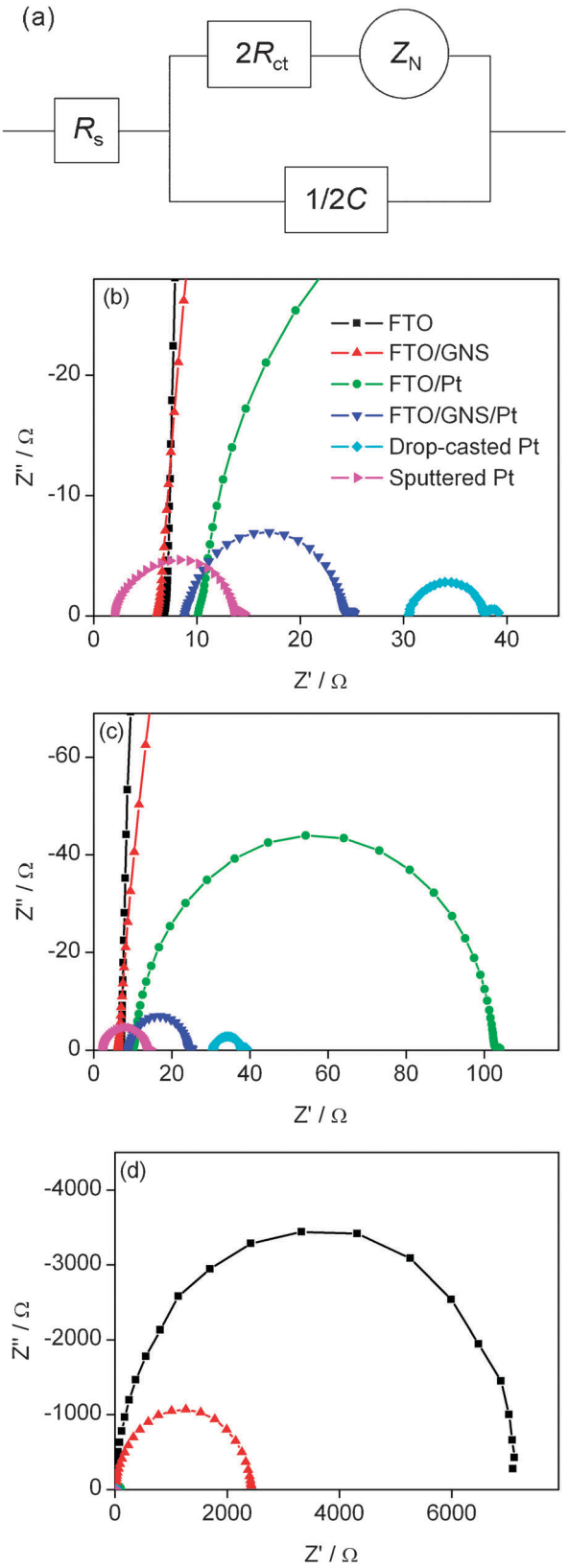

Fig. 3 (a) Equivalent circuit diagram of the symmetric cells consisting of two identical electrodes, R_s: the series resistance, R_{ct}: the charge-transfer resistance, C: double layer capacitance of one electrode, Z_N: Nernst diffusion impedance. (b)–(d) Nyquist plots of EIS at different ranges, measured from 500 kHz to 0.5 Hz at 0 V bias and ac amplitude 10 mV.

remarkably. Although FTO/graphene/Pt has a much smaller Pt loading than the thermally platinized FTO or the sputtered Pt, the former exhibits similar catalytic activity to the latter two electrodes, This result suggests that there is a synergetic interaction between graphene and Pt that can enhance the catalytic activity of the composite film. When Pt particles were supported on graphene, Li *et al.* found an electronic interaction occurring between Pt atoms and the graphene, which leads to electron transfer from the π orbitals of graphene to the d orbitals of Pt atoms.[46] This indicates that graphene not only acts as a supporter, but also plays a direct role in regulating the electronic structure of the Pt nanoparticle during catalytic reactions.[46] Such electronic interaction between Pt atoms and graphene explains why the ultra-thin FTO/graphene/Pt is much better than the graphene or Pt particle film alone and comparable to the thermally platinized FTO or the sputtered Pt in terms of catalytic activity.

The self-assembled GNS, Pt, and GNS/Pt on FTO do not affect the R_s significantly because these films are pretty thin, relative to the case of FTO. For comparison, the drop-casted Pt and sputtered Pt mirror are also studied. The drop-casted Pt exhibits R_{ct} of 3.7 Ω, which is even smaller than that of the sputtered Pt mirror. The drop-casted Pt has a porous structure with fine particles as shown in Fig. 3(e), which is more advantageous to catalytic activity than the bulk Pt for the sputtered case. The sputtered Pt has the smallest R_s (2.0 Ω) due to its metallic character. However, the drop-casted Pt formed by thermal decomposition has R_s of 30.5 Ω, which is much larger than that of FTO. The loose adhesion of thermally decomposed Pt on the FTO surface may be a plausible reason for such high R_s value. Based on the above analysis, the self-assembled FTO/GNS/Pt exhibits comparable catalytic activity to the sputtered Pt mirror and the drop-casted Pt. Its R_s value is a little higher than that for the sputtered Pt mirror but much smaller than that of the drop-casted Pt. The resistance for different CEs is detailed in Table 1.

3.4 Catalytic activity evaluated by CV

The CV measurements offer another means to compare the electro-catalytic property of various electrodes. Fig. 4 shows CV curves of the above symmetrical cells containing the redox electrolyte. Nearly no current could be observed in the potential range of −1.0 to 1.0 V for FTO, indicating that FTO hardly catalyzed the redox reaction of I^-/I_3^- system. Monolayer of graphene was somewhat active to catalyze the redox reactions and small currents were produced. Monolayer of Pt produced larger currents than graphene, suggesting that the former is better than the latter in terms of catalytic activity. The FTO/GNS/Pt produced higher currents than the self-assembled Pt

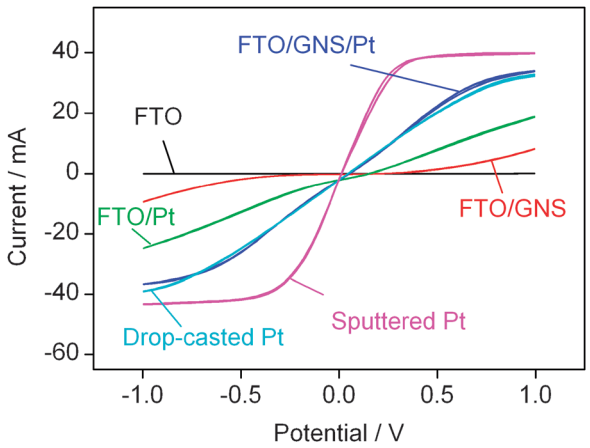

Fig. 4 Cyclic voltammograms of the same symmetric cells as in Fig. 3 under a scan rate of 50 mV/s.

alone, again due to the graphene acting as scaffolds of Pt particles. The FTO/GNS/Pt produced comparable currents as the drop-casted Pt but lower ones than the sputtered Pt. The limiting current changed in the order of sputtered Pt > FTO/GNS/Pt ≈ drop-casted Pt > FTO/Pt > FTO/GNS > FTO. This tendency is consistent with the total resistance (R_s + R_{ct}) estimated from EIS.

3.5 Photovoltaic performance

In order to compare the performance of these CEs in terms of solar cell performance more precisely, thin TiO_2 films (6.0 μm) were used to reduce the errors arising from the thickness difference as possible as we can. The DSSCs constructed with these CEs were tested under illumination of simulated solar light (100 mW cm^{-2}), and the photovoltaic performance data are summarized in Table 1. First, we measured the performance of DSSCs with a sputtered Pt mirror and a drop-casted Pt as the CEs respectively for reference. The DSSC with a sputter Pt as the CE produced η of 6.23% with J_{sc} of 11.22 mA cm^{-2}, V_{oc} of 0.74 V, and FF of 0.75, while the DSSC with a drop-casted Pt as the CE produced η of 4.79% with J_{sc} of 10.91 mA cm^{-2}, V_{oc} of 0.68 V, and FF of 0.65. As expected, the DSSC with FTO as the CE produced very low η of 0.13% with J_{sc} of 3.29 mA cm^{-2}, V_{oc} of 0.56 V, and FF of 0.07. The pretty small value of FF for FTO is ascribed to its large value of R_{ct} as shown in Table 1. Because of the lack of catalytic activity, FTO itself is not qualified for fabrication of efficient DSSCs. When monolayer graphene was used as the CE, the η was improved to 1.85% with J_{sc} of 10.64 mA cm^{-2}, V_{oc} of 0.71 V, and FF of 0.25. The FF is still very low due to its large R_{ct} value related to catalytic activity. It is impressive that the

Table 1 Photovoltaic performance parameters of the DSSCs with different CEs and EIS parameters of the symmetric cells with two identical CEs

CE	V_{oc}/V	J_{sc}/mA cm^{-2}	FF	η/%	R_s/Ω	R_{ct}/Ω	(R_s+R_{ct})/Ω
FTO	0.56 ± 0.02	3.29 ± 0.01	0.07 ± 0.01	0.13 ± 0.01	6.8 ± 0.1	3553.0 ± 30	3559.8
FTO/GNS	0.71 ± 0.01	10.64 ± 0.01	0.25 ± 0.02	1.85 ± 0.08	6.1 ± 0.2	1212.0 ± 15	1218.1
FTO/Pt	0.68 ± 0.01	11.29 ± 0.00	0.62 ± 0.01	4.76 ± 0.06	10.1 ± 0.2	46.4 ± 1	56.5
FTO/GNS/Pt	0.73 ± 0.00	11.42 ± 0.05	0.73 ± 0.00	6.09 ± 0.04	8.8 ± 0.1	7.7 ± 0.1	16.5
Drop-casted Pt	0.68 ± 0.01	10.91 ± 0.08	0.65 ± 0.01	4.79 ± 0.02	30.5 ± 0.2	3.7 ± 0.2	34.2
Sputtered Pt	0.74 ± 0.01	11.22 ± 0.03	0.75 ± 0.00	6.23 ± 0.01	2.0 ± 0.00	5.8 ± 0.1	7.0

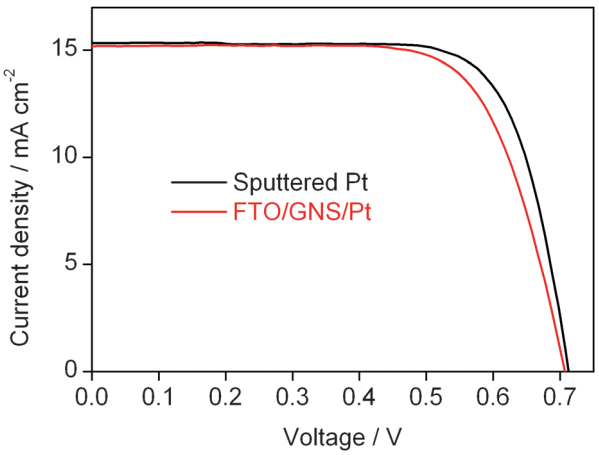

Fig. 5 *J–V* characteristics of the DSSCs with different CEs measured at 100 mW cm^{-2} illumination. The thickness of TiO_2 film was 15 μm.

J_{sc} and V_{oc} values obtained from the monolayer graphene as the CE are just a little lower than those obtained from the sputtered Pt as the CE but comparable with those obtained from the drop-casted Pt as the CE. When the CE changed from FTO/GNS to FTO/Pt film, FF was improved from 0.25 to 0.62 due to the significantly decreased R_{ct}. The self-assembled FTO/Pt is comparable with the drop-casted Pt in terms of power conversion efficiency, but the Pt content in the former is only one sixtieth that in the latter. This indicates that the self-assembled Pt is superior to the drop-casted Pt for use as CE from the point view of cost. Remarkable improvement could be achieved by using the ultrathin composite film of FTO/GNS/Pt as the CE, which produced η of 6.09% with J_{sc} of 11.42 mA cm^{-2}, V_{oc} of 0.73 V, and FF of 0.73. Evidently, the self-assembled FTO/GNS/Pt film is more efficient than the drop-casted Pt and comparable to the sputtered Pt in terms of solar cell performance.

According to Table 1, there is no clear correlation between FF and R_s, but an evident correlation between FF and the total resistance can be derived. Fig. S2 shows the plot of FF against the total resistance. FF decreased with increasing the total resistance. Therefore, a low total resistance is desirable for high FF. In addition, there is no distinct correlation between the resistance and J_{sc} or V_{oc}.

When thick TiO_2 films were used, the DSSCs with FTO/GNS/Pt and a sputtered Pt mirror still generated similar power conversion efficiency. The current–voltage characteristics of DSSCs with thicker TiO_2 films are compared in Fig. 5. The DSSC with a sputtered Pt mirror produced η of 8.16% with J_{sc} of 15.33 mA cm^{-2}, V_{oc} of 0.71 V, and FF of 0.75, while the DSSC with an FTO/GNS/Pt film produced η of 7.66% with J_{sc} of 15.20 mA cm^{-2}, V_{oc} of 0.71 V, and FF of 0.71. As compared to the recently reported Pt nanoparticles as the CE in DSSCs,[47] our electrode shows much higher J_{sc} and FF. In view of its three-order lower Pt amount and much more simple manufacturing technology than the sputtered Pt, the self-assembled FTO/GNS/Pt has gigantic advantage over the sputtered Pt for massive production of DSSCs with low cost. The GNS inserted between FTO layer and Pt layer plays a significant role in achieving good solar cell performance. The graphene not only remarkably increases the availability of Pt particles for electron transfer, but also provides excellent mass transport of reactants to the electrocatalyst Pt.[36] In addition, graphene nanostructures serve as scaffolds to well disperse Pt particles and regulate the electronic structure of the Pt nanoparticle, resulting in efficient catalysis to the reduction of I_3^- ions.[46] If the R_s and R_{ct} can be reduced further, FF and η will be improved further. We tried to fabricate multilayer films of FTO/(GNS/Pt)$_n$ for use as CE and hoped to get better performance. Unfortunately, the multilayer film did not improve the performance. It is reasonable that the Pt directly exposed to the electrolyte is more effective than the inner one for catalysis.

4. Conclusions

In summary, we report a facile approach of fabricating a low-cost and high-performance CE consisting of monolayer graphene/Pt through self-assembly of polyelectrolyte, graphene and H_2PtCl_6 subsequently followed by annealing. The DSSC with the monolayer GNS/Pt as CE achieved a 7.66% power conversion efficiency, which was comparable to 8.16% obtained from the sputtered Pt as CE. The ultrathin self-assembled CE not only contains a little amount of Pt but also can be fabricated using a very simple technology, thus reducing the cost of CE remarkably. This technique is well-suited for flow-line manufacture of CE and facilitates massive production of DSSCs. Another advantage of the self-assembled CE is its transparency, which is advantageous to fabrication of efficient tandem DSSCs. The study on tandem DSSCs with these transparent self-assembled films is now under way.

Acknowledgements

This work was financially supported by the National Basic Research Program (2011CB933302) of China, National Natural Science Foundation of China (20971025, 90922004), Shanghai non-governmental international cooperation program (10530705300), Shanghai Leading Academic Discipline Project (B108), the Project sponsored by SRF for ROCS, SEM, and Jiangsu Major Program (BY2010147).

References

1 B. O'regan and M. Grätzel, *Nature*, 1991, **353**, 737.
2 Q. L. Huang, G. Zhou, L. Fang, L. P. Hu and Z. S. Wang, *Energy Environ. Sci.*, 2011, **4**, 2145.
3 Z.-S. Wang, N. Koumura, Y. Cui, M. Miyashita, S. Mori and K. Hara, *Chem. Mater.*, 2009, **21**, 2810.
4 M. Grätzel, *Inorg. Chem.*, 2005, **44**, 6841.
5 J. H. Wu, S. C. Hao, Z. Lan, J. M. Lin, M. L. Huang, Y. F. Huang, L. Q. Fang, S. Yin and T. Sato, *Adv. Funct. Mater.*, 2007, **17**, 2645.
6 C. H. Yoon, R. Vittal, J. Lee, W. S. Chae and K. J. Kim, *Electrochim. Acta*, 2008, **53**, 2890.
7 C. Y. Lin, J. Y. Lin, C. C. Wan and T. C. Wei, *Electrochim. Acta*, 2011, **56**, 1941.
8 N. Papageorgiou, W. F. Maier and M. Gratzel, *J. Electrochem. Soc.*, 1997, **144**, 876.
9 K. Imoto, K. Takahashi, T. Yamaguchi, T. Komura, J. Nakamura and K. Murata, *Sol. Energ. Mat. Sol. C.*, 2003, **79**, 459.
10 J. K. Chen, K. X. Li, Y. H. Luo, X. Z. Guo, D. M. Li, M. H. Deng, S. Q. Huang and Q. B. Meng, *Carbon*, 2009, **47**, 2704.

11 T. N. Murakami, S. Ito, Q. Wang, M. K. Nazeeruddin, T. Bessho, I. Cesar, P. Liska, R. Humphry-Baker, P. Comte, P. Péchy and M. Grätzel, *J. Electrochem. Soc*., 2006, **153**, A2255.
12 K. X. Li, Y. H. Luo, Z. X. Yu, M. H. Deng, D. M. Li and Q. B. Meng, *Electrochem. Commun*., 2009, **11**, 1346.
13 Z. Huang, X. Liu, K. Li, D. Li, Y. Luo, H. Li, W. Song, L. Chen and Q. Meng, *Electrochem. Commun*., 2007, **9**, 596.
14 G. Calogero, F. Bonaccorso, O. M. Marago, P. G. Gucciardi and G. D. Marco, *Dalton Trans*., 2010, **39**, 2903.
15 G. Veerappan, K. Bojan and S. W. Rhee, *ACS Appl. Mater. Interfaces*, 2011, **3**, 857.
16 E. Ramasamy, W. J. Lee, D. Y. Lee and J. S. Song, *Electrochem. Commun*., 2008, **10**, 1087.
17 W. J. Lee, E. Ramasamy, D. Y. Lee and J. S. Song, *ACS Appl. Mater. Interfaces*, 2009, **1**, 1145.
18 S. H. Seo, S. Y. Kim, B. K. Koo, S. I. Cha and D. Y. Lee, *Langmuir*, 2010, **26**, 10341.
19 J. Han, H. Kim, D. Y. Kim, S. M. Jo and S. Y. Jang, *ACS Nano*, 2010, **4**, 3503.
20 H. Choi, H. Kim, S. Hwang, Y. Han and M. Jeon, *J. Mater. Chem*., 2011, **21**, 7548.
21 J. D. Roy-Mayhew, D. J. Bozym, C. Punckt and I. A. Aksay, *ACS Nano*, 2010, **4**, 6203.
22 L. Kavan, J. H. Yum and M. Grätzel, *ACS Nano*, 2011, **5**, 165–172.
23 P. Hasin, M. A. Alpuche-Aviles and Y. Y. Wu, *J. Phys. Chem. C*, 2010, **114**, 15857.
24 J. B. Xia, N. Masaki, K. J. Jiang and S. Yanagida, *J. Mater. Chem*., 2007, **17**, 2845.
25 K. M. Lee, P. Y. Chen, C. Y. Hsu, J. H. Huang, W. H. Ho, H. C. Chen and K. C. Ho, *J. Power Sources*, 2009, **188**, 313.
26 S. Ahmad, J. H. Yum, H. J. Butt, M. K. Nazeeruddin and M. Grätzel, *ChemPhysChem*, 2010, **11**, 2814.
27 S. Akhtar, Y. S. Kim, O. B. Yang and H. S. Shin, *J. Phys. Chem. C*, 2010, **114**, 4760.
28 J. Zhang, T. Hreid, X. X. Li, W. Guo, L. P. Wang, X. T. Shi, H. Q. Su and Z. B. Yuan, *Electrochim. Acta*, 2010, **55**, 3664.
29 H. C. Sun, Y. H. Luo, Y. D. Zhang, D. M. Li, Z. X. Yu, K. X. Li and Q. B. Meng, *J. Phys. Chem. C*, 2010, **114**, 11673.
30 Q. H. Li, J. H. Wu, Q. W. Tang, Z. Lan, P. J. Li, J. M. Lin and L. Q. Fan, *Electrochem. Commun*., 2008, **10**, 1299.
31 J. H. Wu, Q. H. Li, L. Q. Fan, Z. Lan, P. J. Li, J. M. Lin and S. C. Hao, *J. Power Sources*, 2008, **181**, 172.
32 G. Q. Wang, R. F. Lin, Y. Lin, X. P. Li, X. W. Zhou and X. R. Xiao, *Electrochim. Acta*, 2005, **50**, 5546–5552.
33 K. C. Huang, Y. C. Wang, R. X. Dong, W. C. Tsai, K. W. Tsai, C. C. Wang, Y. H. Chen, R. Vittal, J. J. Lin and K. C. Ho, *J. Mater. Chem*., 2010, **20**, 4067.
34 A. K. Geim and K. S. Novoselov, *Nat. Mater*., 2007, **6**, 183.
35 D. Li, M. B. Müller, S. Gilje, R. B. Kaner and G. G. Wallace, *Nat. Nanotechnol*., 2008, **3**, 101.
36 B. Seger and P. V. Kamat, *J. Phys. Chem. C*, 2009, **113**, 7990.
37 R. Kou, Y. Y. Shao, D. H. Wang, M. H. Engelhard, J. H. Kwaka, J. Wang, V. V. Viswanathan, C. M. Wang, Y. H. Lin, Y. Wang, I. A. Aksay and J. Liu, *Electrochem. Commun*., 2009, **11**, 954.
38 L. F. Dong, R. R. S. Gari, Z. Li, M. M. Craig and S. F. Hou, *Carbon*, 2010, **48**, 781.
39 K. Zhang, Q. L. Yue, G. F. Chen, Y. L. Zhai, L. Wang, H. S. Wang, J. S. Zhao, J. F. Liu, J. B. Jia and H. B. Li, *J. Phys. Chem. C*, 2011, **115**, 379.
40 W. Hummers and R. Offeman, *J. Am. Chem. Soc*., 1958, **80**, 1339.
41 N. I. Kovtyukhova, P. J. Ollivier, B. R. Martin, T. E. Mallouk, S. A. Chizhik, E. V. Buzaneva and A. D. Gorchinskiy, *Chem. Mater*., 1999, **11**, 771.
42 Z.-S. Wang, T. Sasaki, M. Muramatsu, Y. Ebina, T. Tanaka, L. Z. Wang and M. Watanabe, *Chem. Mater*., 2003, **15**, 807.
43 A. Hauch and A. Georg, *Electrochim. Acta*, 2001, **46**, 3457.
44 Z.-S. Wang, H. Kawauchi, T. Kashima and H. Arakawa, *Coord. Chem. Rev*., 2004, **248**, 1381.
45 T. Herricks, J. Y. Chen and Y. N. Xia, *Nano Lett*., 2004, **4**, 2367.
46 W. Qin and X. Li, *J. Phys. Chem. C*, 2010, **114**, 19009.
47 G. Calogero, P. Calandra, A. Irrera, A. Sinopoli, I. Citro and G. Di Marco, *Energy Environ. Sci*., 2011, **4**, 1838.

